1   # Effect of retarders on the early hydration mechanisms of calcium-

2   # sulpho-aluminate (CSA) type cements

3   Maciej Zajac, Jan Skocek, Frank Bullerjahn, Mohsen Ben Haha[(*)]

4   Heidelberg Technology Center GmbH , Rohrbacher Str. 95, 69181 Leimen, Germany
5

6   [(*)]Corresponding author, Tel.:+49 6221 481 13675, E-mail address: mohsen.ben.haha@htc-gmbh.com

7

8   **Abstract**

9   The retardation of calcium-sulpho-aluminate (CSA) type cements by three common retarders – sodium

10   gluconate, sodium-potassium tartrate and borax is investigated. The results show that each of the

11   retarder has a different effect on the early-age hydrates assemblage as shown by quantitative X-ray

12   diffraction, thermogravimetric analysis, scanning electron microscopy and pore solution analysis.

13   Regardless the retarder used, the hydration starts with the formation of ettringite and of some X-ray

14   amorphous hydrates. The ettringite-forming reaction is delayed specifically, depending on the retarder

15   used. The results showed that the retardation is caused either by calcium complexation preventing

16   hydrates formation or surface adsorption of inhibitors or by the formation of a semipermeable layer on

17   the cement grains in the case of tartrate and gluconate. Borax retards the hydration by lowering the

18   initial pH that destabilizes ettringite. Furthermore, the morphology of ettringite is altered depending on

19   the type of the retarder used.

20

21   **Keywords:** Sulfoaluminate (D), Pore solution (B), Retardation (A), SEM (B), X-ray Diffraction (B)

22

1. Introduction

In recent years, calcium-sulpho-aluminate cements (CSA) [1], [2] have attracted the attention of scientists [3] [4] as well as of industry [5] [6] [7] [8]. In general, this type of cements may exhibit broadly similar performance as the ordinary Portland cements (OPC), such as good early and late strength, good protection of steel reinforcement from corrosion and controllable volume stability [1] [4] [9]. However, the CSA cements can achieve even higher strengths at early age while keeping the compressive strength at 28 days comparable to that of a standard OPC [10]. In addition, a very good resistance to sulphate-rich environments has been reported [11]. Besides these technical advantages, the production of CSA clinkers has attracted interest as it generates lower CO_2 emissions than the production of the OPC clinker [6] [12]. For those reasons, CSA type cements represent an interesting and promising alternative to the traditional Portland cements.

The mechanism of a CSA cement hydration depends mainly on the cement clinker composition [13] [14], the amount and reactivity of the added calcium sulphate [15] [16] and on the processing conditions [17]. In comparison to the OPC, the CSA cement reacts faster and most of the hydration heat is released between 2 and 12 h [18], [19]. The primary hydration products are ettringite and monosulphate formed together with amorphous aluminium hydroxide. Depending on the clinker and cement composition, various other hydrates such as strätlingite, C–S–H, monocarboaluminate or hydrogarnet may also precipitate [7], [13], [18], [20], [21].

The fast reaction of the CSA-type cements often requires the use of a retarder to obtain a sufficient open time [1], [22], [23]. Hydroxylic organic compounds such as sugars or citric, tartaric or gluconic acids and their salts are powerful retarders in high alumina cements or calcium alumina cements [24] [25]. It was shown that citric acid [26], [27] and gluconate [28] efficiently retard the early hydration reactions, such as the ettringite formation in CSA - anhydrite - OPC ternary binders. Carboxylic acids can bind to calcium ions on the crystal surfaces and prevent further growth on these surfaces [29]. Citrate and tartrate ions are also powerful chelators of solution Ca^{2+} and Al^{3+} and would be expected to influence the nucleation and growth of phases containing these ions [29]. Similarly, sugars are capable of complexing calcium and possibly also aluminium since they contain numerous hydroxyl groups that deprotonate to form multidentate, negatively charged molecules, which in turn tightly bind positively charged solution ions [29]. Effect of these compounds on the hydration of the CSA and of the OPC is qualitatively comparable. However, chloride salts, which are powerful accelerators in OPC, normally have retarding effects in CSA, somewhat depending on dosage and temperature [25], [30]. Another inorganic retarder applied for CSA

54 type cements is Borax (sodium tetraborate) [10], [31]. Both boric acid and its sodium salt inhibited the

55 nucleation of ettringite, but instead allowed six-sided plates of the metastable AFm phase to form [29].

56 To better understand the hydration mechanisms of CSA cements in the presence of different retarders,

57 the composition of the solid and the liquid phase during hydration of two CSA cements was followed.

58 The ionic composition of the liquid phase was linked to the precipitation of hydrates, which control the

59 setting, hardening and the evolution of the early mechanical properties. The focus of this study is on the

60 evolution of the properties at the early times, i.e. at times lower than 7 days of hydration. The effects of

61 three retarders with supposedly different ways of retardation were investigated: sodium gluconate

62 (labelled G, $NaC_6H_{11}O_7$), tartrate (T, $(K,Na)_2C_4H_4O_6 \cdot 4H_2O$) and borax (B, $Na_2B_4O_7H_2O_8$).

63 In the paper the cement notation is used: C = CaO, S = SiO_2, A = Al_2O_3, F = Fe_2O_3, $\bar{S}$ = SO_3, N = Na_2O, K =

64 K_2O.

65 ## 2. Materials

66 CSA clinker and natural anhydrite (AH) were used to prepare the cements. The chemical composition as

67 determined by the XRF is given in **Table 1**. The mineralogical composition determined by the quantitative

68 XRD Rietveld analysis is given in **Table 2.**

69 The particle size distributions of ground clinker (C) and anhydrite determined by laser granulometry

70 using a Malvern Mastersizer 2000 (Fraunhofer model, propanol-2-ol (dispersant)) are given in **Figure 1.**

71 The experimental matrix is given in Table 3. Two cements were prepared: ground clinker (labelled C) and

72 ground clinker blended with 10 wt.-% of the anhydrite in a laboratory mixer (labelled CAH). The

73 experiments were conducted at the water to cement (W/C) ratio of 2.0. Performing the hydration study

74 at the high W/C ratio allowed performing the pore solution analyses and the phase assemblage

75 investigations on a single sample even at 7 days of hydration. The retarders were pre-dissolved in the

76 mixing water (deionized). This procedure assured a homogeneous distribution of the retarder in the

77 sample as well as an easy and reproducible sample preparation. The retarders' solutions were added on

78 top of the cement mass, i.e. the mass of the retarders was not included in the W/C ratios.

79 Additional samples were prepared at W/B =0.5 for microstructural investigations by SEM.

3. Methods

To investigate the hydration of the two cements, all sample preparations and investigations were carried out at 20 °C if not stated otherwise.

A conduction calorimeter (Thermometric TAM Air) was used to determine the rate of hydration heat release during the first 7 days. 6.0 g of cement was weighed into a flask and the corresponding amount of retarder solution was added and mixed externally for about 1 minute before inserting the sample into the calorimeter.

For the X-ray diffraction (XRD), thermogravimetric (TGA) and pore solution analyses, about 50 g of cement was mixed with the retarder solution in a plastic container. A single sample was prepared for each time investigated. The cement pastes were mixed using a laboratory mixer. The plastic containers were stored sealed. During the curing time, samples were regularly shaken. The pore solutions were obtained by a pressure-filtration using a 0.45 μm Nylon filter. For further analyses, one part of the solution was diluted by 1:20 with deionized water to prevent any precipitation of solids. The total concentrations of elements were determined using inductively coupled plasma optical emission spectroscopy (ICP-OES Varian Vista-Pro). The other part of the pore solution (i.e. as extracted, not diluted) was used for pH measurements. The pH electrode was calibrated against KOH solutions of known concentrations. The measurements were performed not later than 2 hours after the solution extraction. For the XRD and the TGA measurements, the samples were ground and the hydration was stopped by solvent exchange with isopropanol for 15 min followed by flushing with diethyl ether. TGA/DTG (NETZSCH STA F449 F3 Jupiter) was carried out on 30±2 mg of the stopped cement paste. Open vessels in N_2 atmosphere and a heating rate of 20 °C/min up to 1050 °C were used.

The quantitative phase compositions of the unhydrated cements and of cement pastes were evaluated using the XRD analysis coupled with the Rietveld refinement method. The XRD patterns were obtained at room temperature (24±2 °C) using Bruker D-8 Advance in a θ-2θ configuration with a monochromatic CuKα radiation (λ = 1.54059 Å) and equipped with the LYNXEYE (1-d) detector. The generator settings were 40 kV and 40 mA. The measurement range was 5° to 70° 2θ with a step-size of approximately 0.02°. 10 wt.-% of zincite (ZnO) was added as the internal standard. A more detailed description of the test procedure used is available in [17].

Additional samples were prepared for the microstructure observations. The cement pastes were prepared at W/C = 0.5 using the same solutions as for the samples prepared at W/C = 2.0. The fragments

110 of cement pastes were immersed in isopropanol and subsequently dried at 40 °C for 24 h. The fractured

111 surfaces of the samples were gold coated and examined using Hitachi S450 scanning electron microscope

112 (SEM).

113 For the calculation of the supersaturating indexes, GEMS-PSI, a geochemical speciation code [32],

114 involving a thermodynamic database [33] [34] which has been updated with the cement-specific data

115 [35] [36] was used.

116 ## 4. Results

117 ### *4.1. Hydration of the reference samples*

118 #### *4.1.1. Kinetics of hydration*

119 The results of the isothermal conduction calorimetry are shown in Figure 2. Heat flow curves differ for

120 the two investigated reference samples. Both reference cements show a very short induction period

121 after the initial peak. After that, sample C is characterized by three overlapping peaks with their maxima

122 at 2.5 h, 4.7 h and 53 h, respectively. The peak at 4.7 h has a shoulder after its maximum. Sample CAH

123 shows the main hydration peak at 5.5 h with a shoulder at 3.5 h. The later peak(s) were not observed up

124 to 7 days of hydration. The multi-peak evolution of the heat release is consistent with former studies

125 [18] [14] [16].

126 The cumulative heat, as shown in Figure 3, agrees very well with the evolution of the hydration degree of

127 cement clinker, calculated based on the Rietveld quantification (Figure 8). In general, the cumulative

128 heat is believed to be proportional to the hydration degree of hydraulic cement [14] [25]. In the case of

129 the reference samples, a substantial degree of hydration is already observed after 30 minutes. Between

130 30 minutes and about 2 hours, the hydration progresses slowly. The hydration significantly accelerates

131 between 2 and 10 hours. After 10 hours, the hydration slows down again. After 10 hours, the C sample

132 shows a faster hydration than CAH.

133 Table 4 and 5 depict the dissolution of major cement clinker phases in C and CAH samples. It is seen that

134 the fast progress of the hydration between 2 and 10 hours is related to the dissolution of aluminium

135 bearing phases, i.e. $C_4A_3\bar{S}$, CA and C_4AF that react fast with water and the available sulphate [13] [18].

136 The XRD and TG data suggest that a significant amount of $C_4A_3\bar{S}$ reacts during the first 30 minutes in

137   samples C and CAH (first measurement point, see as well Figure 9). Both cements contain anhydrite. In

138   the samples C, anhydrite is not detectable after 4 h of hydration. In the CAH sample, about a half of the

139   anhydrite reacts up to the first day of hydration. At 7 days, anhydrite is no more detectable. Belite reacts

140   significantly slower than the aluminate bearing phases during the investigated period [19].

141   ### 4.1.2. Hydrates assemblage

142   Rietveld calculations were performed to follow the evolution of the ettringite content as well as the

143   content of the XRD – amorphous hydrates in the investigated samples. AFm and strätlingite were

144   considered as parts of the amorphous phase due to their low level of crystallinity. The XRD data shown in

145   Figure 4,5 and9 show that ettringite is the main hydration product at early times. The XRD results are

146   confirmed by the TGA data (Figure6 and7). In C and CAH samples, substantial amounts of ettringite are

147   formed already after 30 minutes. This is in agreement with the qualitative analysis of the XRD and DTG

148   data (Figure 9). It is noticeable that almost the same amount of ettringite is formed up to 2 hours. The

149   ettringite content increases slowly up to 2 hours and 3 hours for C and CAH, respectively. Afterwards, the

150   ettringite formation accelerates and reaches its final content at around 1 day. The final ettringite content

151   is considerably higher in the sample CAH when compared to the sample C. This is obviously a result of

152   the additional anhydrite. The evolution of the XRD amorphous phase content (Table 4 and 5 follows the

153   trend shown for the hydration degree (Figure 8). The nature of hydrates cannot be exactly identified

154   either form the XRD or TGA results. The corresponding broad and flat weight loss between 200 °C and

155   400 °C could be related to the presence of several phases like AFm, strätlingite and aluminium hydroxide.

156   The XRD data, in agreement with the TGA data, suggest that the content of these phases is considerably

157   higher in the samples C than in the CAH samples at 1 day and later.

158   Figure 10 shows the SEM images of the fractured samples after 1 day. In the CAH sample, ettringite

159   intermixed with aluminium hydroxide is visible confirming that the ettringite is the main hydration

160   product. Needles of ettringite display a range of sizes – from large needles with cross-sections up to 5

161   µm down to needles with cross-sections in the range of tenths of µm. The needles have irregular shape.

162   Ettringite in sample C had a similar morphology. However, only CAH samples are presented due to their

163   higher ettringite contents allowing an easier comparison of the effects of retarders on the ettringite

164   morphology.

4.1.3. Pore solution chemistry

The results obtained from the chemical analyses of the extracted pore solutions, i.e. elemental concentrations (Ca, Al, S, Si, Fe and alkalis) and pH, are presented in Table 6 and 7 . For the reference samples and the investigated period, the pore solution concentration is dominated by alkalis, calcium, aluminium and sulphate. Silica and iron concentrations are under detection limits for both samples. Sodium and potassium concentrations are relatively stable over the studied period. The calcium concentration decreases rapidly from ~17 mmol/l at 5 minutes to less than 1 mmol/l at 1 day. After that, the calcium concentration is relatively stable. The sulphate concentration (strictly speaking, the sulphur concentration is measured by the ICP) decreases over the hydration time from 50 mmol/l to 0.1 mmol/l in the case of C and to ~2 mmol/l in the case of CAH cement after 7 days. Aluminium concentration increases initially, up to 8 hours and 4 hours for C and CAH, respectively, reaching ~60 mmol/l. Then the aluminium concentration starts to decrease. The pH of the cement pore solution is close to 11 at the beginning of the hydration and increases up to 13. In the sample CAH, the pH reaches a lower level confirming that the pH is reversibly proportional to the concentration of sulphate. Winnefeld al. [13] and Li et al. [20] analysed the liquid phase of reacting CSA cements. Their results show similar concentrations of Ca and sulphate as well as similar trends as presented here, i.e. the drop of both concentrations during the course of hydration, despite the differences in the experimental approach. They also report the increase of aluminium concentration followed by the drop after some time. Contrary to their experiments, the continuing increase of the alkalis concentration was not observed, probably due to the higher W/B ratio used here.

A closer analysis of the pore solution results revealed that the charge balance is not exact. This can be expected since the measurements of alkali and alumina with ICP are associated with considerable errors of measurements. Moreover, a carbonation of the solutions during pH measurements cannot be fully acoided [37].

4.2. Effect of Tartrate

4.2.1. Kinetics of hydration

The addition of tartrate has a pronounced effect on the hydration kinetics. Tartrate-retarded system produces a small peak around 5.5 hours after the initial dissolution peak followed by a very low heat flow for C-T and CAH-T samples (Figure 2). The characteristic multi-peak heat evolution seen for the reference

194   sample is not visible. Figure 3 reveals that the dormant period is strongly prolonged; hydration is strongly

195   accelerated only after about 4 h. At 7 days, the hydration degrees of reference samples and samples with

196   tartrate are similar. However, the cumulative heat is significantly lowered. QXRD data (Table 4 and 5)

197   reveal that tartrate strongly retards the hydration of ye'elimite and the dissolution of anhydrite.

198   Nevertheless, ye'elimite and gypsum are fully consumed after 7 days of reaction. The data suggest that

199   also the hydration of C_4AF is retarded.

4.2.2. Hydrates assemblage

201   In C-T sample, tartrate delays the formation of ettringite; it is firstly detected after 8 hours (Figure 4 and

202   Table 4). The formation of strätlingite is observed after 7 days by the XRD and TG (Figure 6), whereas no

203   AFm phase could by detected by means of the XRD analysis. In the case of CAH samples mixed with the

204   tartrate solution, similar phenomena are observed: tartrate delays the formation of hydrates. Later on,

205   the crystalline hydrates assemblage is similar as for the reference sample CAH, however, at 7 days, small

206   reflexion of strätlingite are visible in the XRD. The TGA data shown in Figure 7 confirms that the main

207   hydration product of the CAH-T system is ettringite and aluminium hydroxide.

208   Microstructure observations reveal that in the CAH-T sample, similarly to the CAH sample, the ettringite

209   needles of various sizes are intermixed with AH_3. The shape of the needles is, however, better defined

210   showing the typical hexagonal crystals. The smallest needles observed in the CAH sample, are not

211   present in the CAH-T.

4.2.3. Pore solution chemistry

213   Tartrate has a similar effect on the pore solution concentration in both two investigated cements.

214   Tartrate results in higher calcium and sulphate concentrations than in the reference samples up to one

215   day of hydration. These two concentrations decrease over time. At the beginning of hydration, the

216   concentration of aluminium is very low <0.01 mmol/l and it increases rapidly between 4th and 8th hour of

217   hydration reaching ~40 mmol/l. Afterwards, up to 7 days, the aluminium concentration decreases. Since

218    $(K,Na)_2C_4H_4O_6 \cdot 4H_2O$ was used in this study, the initial sodium and potassium concentrations are higher as

219   is also the pH. Additionally, in the sample CAH-T, the concentration of silicon increases above the

220   detection limit up to ~0.03 mmol/l.

4.3. Effect of borax.

4.3.1. Kinetics of hydration

The addition of borax results in a similar shape of the calorimetry curves of both cements as shown in Figure 2. The main hydration peak starts after 24 hours and have its maximum at 33 hours. However, the heat flow increases already after 12 hours of reaction. The cumulative heat (Figure 2) as well as the hydration degree evolution (Figure 8) shows that borax strongly retards the hydration up to one day. After that, the hydration proceeds significantly faster than for the references. Between 1 and 2 days, the hydration degree of borax samples reaches the level of reference samples and evolves similarly to them up to 7 days.

4.3.2. Hydrates assemblage

Borax retards the formation of XRD-detectable hydrates up to one day of hydration (Figure 4 and 5, Table 4 and 5). Instead, the precipitation of gypsum is observed. Between 1 and 2 days, a massive formation of ettringite and strätlingite is observed in addition to the depletion of gypsum. At 7 days, the difference between C-B and CAH-B samples is similar as the difference between C and CAH samples, respectively. In the C-B samples, a massive formation of AFm phases is observed whereas in the sample CAH-B, ettringite and alumina hydroxide are the main hydration products (Figure 6 and 7).

The morphology of ettringite of the CAH-B sample (Figure 10) differs significantly when compared to the reference and the tartrate-retarded sample. Contrary to both CAH and CAH-T, the range of ettringite sizes is much narrower; all needles have their cross-section within ~0.1 and 1 µm. Ettringite needles have a well-defined shape.

4.3.3. Pore solution chemistry

The addition of borax results in an increase of the initial concentrations of calcium, sulphate and silicon for both investigated samples as shown in Table 6 and 7. The calcium and sulphate concentrations drop significantly after the first day of hydration. Aluminium concentration stays below the detection limit. Only at 2 days, an increased aluminium concentration was detected. Boron concentrations are initially high at around 120 mmol/l. They decrease slowly up to one day and then drop to values below 0.01 mmol/l already at 2 days. This time correlates with the increase of the aluminium concentration and with the sharp decrease of the calcium concentration. The addition of borax results in a significant drop

249 of the initial pH when compared to the reference samples. The pH is reversibly proportional to the boron

250 concentration. The measured sodium concentrations are comparable to the reference samples. These

251 are unexpected results since sodium was released from borax. Theoretically, the sodium ion

252 concentration needs to be approximately half of the borate concentration. This assumption was

253 confirmed by measurements of the concentrations in the solutions used for sample preparation. The

254 measured concentration of sodium and boron in this solution was 50 mmol/l and 115 mmol/l

255 respectively. Consequently, the very initial concentration of sodium in C-B and CAH-B samples around

256 65–70 mmol/l should be expected accounting for the alkalis from cement. However, in both investigated

257 cements, i.e. C-B and CAH-B, the sodium concentration is similar to the reference samples. The sodium

258 concentrations increase rapidly between the 1st and the 2nd day and drop once more afterwards.

259 ### *4.4. Effect of gluconate*

260 ### *4.4.1. Kinetics of hydration*

261 Gluconate strongly retards the hydration of C and CAH cements (Figure 2). After the first dissolution

262 peak, only a week activity is observed by the calorimetry. This is confirmed by the evolution of the

263 hydration degree that evolves only slowly during the investigated period.

264 Gluconate retarders the formation of ettringite less than the other investigated retarders; the first

265 ettringite is detectable already after 4 hours (Figure 4 and 5) in C-G, i.e. before the C-T and C-B.

266 According to the XRD, no other crystalline hydrates are present. These results are confirmed by the TGA

267 data shown in Figure 6 and 7. At one day of hydration, ettringite appears as the main hydration product

268 in C-G and CAH-G samples. No significant amounts of AFm or AH$_3$ can be detected. At 7 days, the TGA

269 reveals a presence of several phases: ettringite, strätlingite, AFm and AH$_3$ in the C-G sample. In the case

270 of CAH-G, ettringite is still the main hydration products. The amount of hydrates is clearly lower than in

271 the reference samples.

272 In the sulfate-rich gluconate-containing sample, CAH-G, large ettringite needles with cross-sections

273 greater than 1 μm are visible. The needles have rectangular cross-sections with aspect ratios of approx.

274 1:3 to 1:1. Partly-dissolved clinker grains as well as the aluminium hydroxide can be identified in the

275 images (Figure 10).

276   ### *4.4.2. Pore solution chemistry*

277   The addition of gluconate results in an increase of the calcium, silicate, alkali and sulphate

278   concentrations when compared to the reference samples (Table 6 and 7). Aluminium concentration is

279   low in the presence of gluconate at 5 min (3 mmol/l) and it increases continuously up to 7 days of

280   hydration, reaching 90 mmol/l for the C-G sample and 30 mmol/l for CAH sample at 7 days. The

281   concentrations of Si and Fe are higher when compared to the other samples. The pH evolution is

282   different as for reference cements. It is initially higher, reaching about 11.8 at 5 minutes and does not

283   significantly change significantly during the experiments.

284   ## 5. Satura ons indices

285   The experimental data of the pore solution concentrations of C and CAH were used to calculate the

286   saturation indices of possible hydrate phases in order to reveal which phases could precipitate. The

287   saturation indexes were not calculated for Si bearing phases (strätlingite, C-S-H) since the Si

288   concentration, in most cases, was under the detection limit.

289

290   Ettringite is always highly oversaturated except for the borax retarded samples at early ages; the degree

291   of oversaturation decreases with time. Additionally, aluminium hydroxide, monosulphate and CAH_{10} are

292   oversaturated up to one day of hydration. Gypsum and portlandite are undersaturated. However, not

293   every oversaturated phase will precipitate. The amount and type of the phase precipitated depends on

294   the kinetic of the precipitation as well as on thermodynamic stability of other phases. The predicted

295   precipitation of ettringite, gypsum, AH_3 and monosulphate is in agreement with data of the solid phase

296   composition. The initially high concentration of calcium, sulphate and alkalis is a result of the very rapid

297   dissolution of readily soluble alkalis (Table 2) and ye'elimite. It demonstrates that at early age, the pore

298   solution concentrations are dominated by the hydration of ye'elimite and calcium aluminate phases with

299   readily soluble sulphates and anhydrite. As a result, ettringite, gibbsite and potentially monosulphate are

300   predicted to precipitate in agreement with the experimental data.

301   The addition of tartrate results in the increase of the calcium and sulphate concentration in the pore

302   solution already after 5 minutes. This is related to the dissolution of the readily soluble alkalis. The pore

303   solution concentrations of Ca^{2+}, $Al(OH)_4^-$ and SO_4^{2-} are limited by the ettringite solubility. The very low

304   concentration of alumina allows further increase of the calcium and sulphate concentrations. The

305   calcium concentration is additionally increased by formation of complexes with tartrate. The high

306 concentrations of calcium and sulphate result in the supersaturation of the pore solution with respect to
307 gypsum. One notes that the solution is supersaturated with respect to ettringite and monosulphate, but
308 undersaturated with respect to alumina hydroxide (Figure 12). These results indicate that the ettringite
309 and monosulphate could precipitate. However, these phases did not form because their nucleation and
310 growth was poisoned by tartrate or because the dissolution of ye'elimite and calcium aluminates was
311 blocked which resulted in the lack of alumina. The high concentration of calcium and sulphate can have a
312 negative role on the dissolution rate of anhydrous calcium aluminates. It was proven that the high
313 concentration of calcium and sulphate slows down the dissolution of calcium aluminate phases in the
314 OPC [38] [39].

315 Due to the low pH in the boron retarded systems and to the low concentration of aluminium, the
316 solution is undersaturated with respect to ettringite and AFm phases (Figure 14). Because of the very
317 high concentration of calcium and sulphate, the dissolution of ye'elimite may be slowed down. However,
318 this cannot be verified since the solubility data for ye'elimite are not available.

319 The slow decrease of the boron concentration may be related to the precipitation of either calcium-
320 boron phases or AFm phases (however, the AFm is modelled to be undersaturated). It is known that
321 boron can substitute for sulphate in the AFm phase [40] [41]. The boron containing AFm may easily form
322 the solid solution with hemicarbonate, which complicates the investigated system even more. In both
323 cases, these phases may precipitate as XRD amorphous explaining the fact that they are not seen by the
324 XRD [51] [37]. However, one notes the significant amount of the XRD amorphous content in the samples
325 C-B and CAH-B (Table 4 and 5). Another possibility of borax absorption is alumina hydroxide. However,
326 data supporting or disproving this hypothesis are not available to authors' knowledge.

327 Once boron is consumed and its pH-buffering effect stops, the pH increases considerably followed by the
328 supersaturation with respect to ettringite. Further hydration proceeds very rapidly. This is confirmed by
329 the high increase of the alumina concentration as well as by the decrease of the sulphate and calcium
330 concentrations between 1 and 2 days of hydration (Table 6 and Table 7). During that time, the phase that
331 bound sodium decomposes which results in an increased sodium concentration. Consequently, the
332 released sodium is reabsorbed on the hydrates formed as discussed for the reference samples.

333 In the gluconate retarded system, the solution is strongly oversaturated with respect to ettringite and
334 monosulphate phases. Such a mechanism is comparable to that of tartrate. However, contrary to the
335 tartrate, portlandite is the only undersaturated phase. All the other phases are close to be saturated or
336 are strongly supersaturated.

6. Discussions on retarda on mechanisms

Three different cement hydration inhibiting mechanisms have been proposed to explain the action of different retarders in cement [25]:

- Calcium complexation that involves either removing calcium from solution by forming insoluble salts or chelating calcium in solution to prevent hydrates formation.
- Surface adsorption of inhibitors directly onto the surface of either the anhydrous or (more likely) the partially hydrated mineral surfaces that blocks future reactions with water.
- Formation of a semipermeable layer on the cement grains that slows the migration of water and extends the induction period.

Tartaric acid is a known calcium chelating ligand with the resulting complex only sparingly soluble in water. The hypothesis that calcium is complexed by the tartrate can be valid since the calcium concentration in the samples C-T and CAH-T is significantly higher than in the reference samples. In addition to the calcium chelating, tartaric acid has a high affinity for aluminium. In moderately acidic solutions, aluminium is capable of coordinating to the octahedral aluminium while the tetrahedral aluminium is preferred in moderately basic solutions. Above pH of 11.5, the tetrahedral aluminium tartrate complex dissociate into the free ligand and $Al(OH)_4^-$ [42]. Bishop and Barron [43] studied mechanisms of the C_3A reaction retardation by the tartrate. They proposed a mechanism in which tartaric acid directly adsorbs onto the surface of hydrating C_3A and blocks by that its reaction with water. The mechanism involves a dissolution of calcium by extraction with tartaric acid (exposing the residual aluminium) followed by a precipitation of a layered calcium tartrate that binds to the surface of the C_3A grains, inhibiting further hydration. On the other hand, Cody [29] noted that tartrate inhibits ettringite nucleation and growth. Additionally, one notes that ettringite in natural or synthesized pore solutions can adsorb high amounts of negatively charged polycarboxylate-based superplasticizers [44] [45]. Since tartrate used in the present study is also negatively charged, it could also adsorb onto ettringite surfaces and block its growth. The results presented in this study does not allow distinguishing whether the tartrate retarders the hydration of CSA cement by limiting the clinker dissolution or by limiting the growth of ettringite. Once the tartrate is consumed, e.g. by the ab- or adsorption on the surface of hydrates during the slow initial hydration, the course of the reaction becomes the same as for the reference samples. The tartrate consumption could be related e.g. to its adsorption to the slowly formed ettringite or to the increase in the pH that became high enough to stabilize the aluminium–tartrate complex.

13

368   The addition of borax results in the low pH of the cement pore solution. The low pH can be associated

369   with the presence of $B(OH)_4^-$ species in the cement pore solution. As the electro-neutrality of the pore

370   solution has to be ensured, the hydroxide concentration decreases and so does the pH. Boric acid is

371   a solid substance soluble in the water — with solubility of 55 g/l at 25 °C. As boron is an electron

372   deficient element, boric acid acts as a weak acid. Below 22 mg/l, mononuclear species $B(OH)_3$ and

373     $B(OH)_4^-$ are present. Polyborates appear at concentrations of boron higher than 1000 mg/l. In the pH

374   range above 7, the mole fraction of $B(OH)_3$ decreases while that of $B(OH)_4^-$ increases with increasing pH.

375   At pH values around 9, the $B(OH)_3$ and $B(OH)_4^-$ concentrations are practically equal, while at higher pH,

376     $B(OH)_4^-$ is the predominant species [46].

377   Additional factor that contributes to the decreased pH is that the sodium concentration is significantly

378   lower when compared to the expected one. Consequently, it is reasonable to assume a formation of

379   a metastable Na-rich phase:

380   •   Sodium can precipitated to form the so called U-phase; i.e. a kind of AFm phase, which can be

381   formed in significant amounts in hydrating CSA cements. However, the formation of the U-phase

382   requires a high pH and a high concentration of the sodium sulphate [47] [48]. None of these

383   conditions is fulfilled in the investigated systems

384   •   Another possibility is a precipitation of the mineral called Dawsonite ($NaAlCO_3(OH)_2$). Dawsonite,

385   however potassium containing, was found in the CAC cements when hardened CAC concrete is

386   exposed to an alkaline environment [49], [50]. Literature data [51], [52], [53], [54] suggest that

387   the optimal experimental conditions to synthesize dawsonite require moderately basic solutions.

388   TGA (Figure 15) data suggest the presence of dawsonite since they are similar to TGA curves of

389   synthetic $NaAlCO_3(OH)_2$ [55]; two characteristic effects are visible: mass loss at 300 °C and

390   575 °C.

391   Dawsonite, or other metastable Na-rich phase, present in the borax-retarded samples, is probably

392   amorphous since it was not detected by the XRD. Amorphous or weakly crystalline Dawsonite has been

393   reported [50] [54]. The TGA data at early times clearly suggest the presence one of this phase as shown

394   in Figure 15. The hypothesis of formation of this phase is supported by the low alumina concentration

395   and by the presence of limestone in the cement clinker (Table 2). Additional supporting argument is the

396   fact that the limestone can rapidly dissolve in the cement pore solution [56] to provide carbonate anions

397   to form Dawsonite.

It is widely recognized that sugars are one of the most effective hydration inhibitors of the hydraulic cements. Based on several results of different studies, it has been hypothesized that saccharide adsorption on hydrating cement particles contributes to their relative effectiveness in slowing the hydration [24] [57] [58] [59] [60]. However, there is no clear explanation of the exact mechanism how the sugars retard. The work of Smith et al. [61] shows that carboxylate-like glucose reacts with the – Al(OH) groups of the calcium aluminium hydrates. This points out a strong adsorption of saccharine acids onto the aluminium hydration products. The gluconate ion is a well-known inhibitor of gibbsite, $Al(OH)_3 \cdot 3H_2O$, precipitation and consequently it was proposed that gluconate might block the growth of the gibbsite [62] [63].

Sugars are capable of complexing calcium and possibly aluminium since they contain numerous hydroxyl groups that deprotonate to form multidentate, negatively charged molecules, which in turn tightly bind positively charged solution ions [29]. Gluconate forms the complexes with the calcium, alumina and iron with stability and composition depends on the pore solution pH [64] [65] [66]. This explains the higher concentration of the calcium and iron in the cement pore solution measured. Additionally, the higher centration of Si can be associated with some complexes with gluconate.

The differences in the rate of ettringite formation and in the pore solution composition during the hydration are probably responsible for the differences in the ettringite morphology observed by the SEM investigations. Before the rapid dissolution of ye'elimite, the already formed ettringite crystals have enough time to grow resulting in large, well-defined crystals. After the acceleration period, a significant amount of ettringite forms over a short time explaining the smaller crystals filling the space between the large crystals.

7. Conclusions

The effect of three different retarders – Na/K-tartrate, Na-gluconate and borax – on the early age hydration of CSA cements was investigated using a multi-method approach. The evolution of solid phases as well as of the pore solution composition was measured between 5 minutes and 7 days. The early hydration of CSA cement is dominated by the ye'elimite hydration whose hydration is further accelerated by the presence of the readily soluble alkalis and calcium bearing phases. The added anhydrite seems to have little impact on the very early hydration. This is most probably related to its low solubility. However, after about two hours of hydration, anhydrite participates in the reaction by stabilizing the ettringite instead of AFm phases. Despite the strong effect of retarders on the CSA cement

15

428 hydration, the aforementioned hydration path is always kept e.g., ettringite is the main hydration
429 product in both C and CAH systems at early age.

430 The retarders have similar effects on the pore solution centration. On the one hand, the calcium and
431 sulphate centration is increased when compared to the neat samples. This is related to the complexing
432 action of the organic additives or lowering of the pH by borax. These high concentrations result in the
433 initial supersaturation of the pore solution with respect to gypsum. In the case of the neat samples, the
434 gypsum is undersaturated after 5 minutes. On the other hand, the alumina concentration is very low.
435 Further common point of all retarders is that the impact of a given retarder on the hydration mechanism
436 is similar for the two investigated cements, i.e. independent of the sulphate added.

437 Nevertheless, there are the differences among the investigated retarders:

438 • Tartrate and gluconate seems to delay the dissolution and / or precipitation and growth
439 • Borax destabilizes the hydrates because of the low pH

440 The main action of the both organic retarders is the slowing down of the hydration kinetics. However,
441 gluconate slows down the reaction much stronger suggesting much stronger interaction with the
442 hydrating cement. The retarders clearly act on the formation of ettringite as revealed by the
443 microstructure observation.

444 In the case of borax, a clearly different retarding effect is observed. Firstly, the addition of borax results
445 in a significant drop of the pH, whereas the additions of tartrate and gluconate resulted in its increase.
446 Borax stops completely the reaction of ye'elimite and other cement clinker phases but not the reaction
447 of anhydrite. As a result, gypsum is the only crystalline phase formed at early age. Some amorphous
448 phases may precipitate as revealed by the TG. The results indicate that a meta-stable sodium-bearing
449 phase precipitates. Borax is gradually consumed from the pore solution. Once its concentration is low
450 enough, the hydration reaction proceeds rapidly.

451 All investigated retarders may work efficiently as the set retarding agents since they supress or slow
452 down the initial formation of ettringite. The correlation between the effect of retarders on the
453 microstructure development and on the evolution of the mechanical performance is a subject of our
454 further studies.

8. Literature

[1]   L. Zhang, M. Su and Y. Wang, "Development of the use of sulfo- and ferroaluminate cements in China," Advances in Cement Research, vol. 11, pp. 15-21, 1999.

[2]   P. K. Mehta, "Investigations on energy-saving cements," World CementTechnology, vol. 11, pp. 166-177, 1980.

[3]   I. Odler, Special Inorganic Cements, London: E&FN Spon, 2000.

[4]   M. Juenger, F. Winnefeld, J. Provis and J. Ideker, " Advances in alternative cementitious binders," Cement and Concrete Research, vol. 41, no. 12, p. 1232–1243, 2011.

[5]   C. Popescu, M. Muntean and J. Sharp, "Industrial trial production of low energy belite cement," Cement & Concrete Composites, vol. 25, p. 689–693, 2003.

[6]   E. Gartner, "Industrially interesting approaches to low CO2 cements," Cement and Concrete Research, vol. 34, pp. 1489-1498, 2004.

[7]   " ALIPRE® web site, ALIPRE® webhttp://www.italcementigroup.com/ENG/Research+and+Innovation/Innovative+Products/Alipre/ site," Visisted Nowember 2014.

[8]   "Aether® web, http://www.aether-cement.eu/," Visited November 2014.

[9]   F. Glasser and L. Zhang, "High-performance cement matrices based on calcium sulfoaluminate– belite compositions," Cement and Concrete Research, vol. 31, p. 1881–1886, 2001.

[10]   J. Pera and J. Ambroise, "New applications of calciumsulfoaluminate cement," Cement and Concrete Research, vol. 33, no. 3, pp. 371-676, 2003.

[11]   S. Ioannou, K. Paine and K. Quillin, "Strength and durability of calcium sulfoaluminate based concretes," in 12th International Conference on Nonconventional Materials and Technologies NOCMAT, Cairo, Egipt, 2010.

[12]   C. Popescu, M. Muntean and J. Sharp, "Industrial trial prodcution of low energy belite cement," Cement and Concrete Composites, vol. 25, pp. 689 - 693, 2003.

[13]   F. Winnefeld and B. Lothenbach, "Hydration of calcium sulfoaluminate cements — Experimental findings and thermodynamic modelling," Cement and Concrete Research, vol. 40, p. 1239–1247, 2010.

486 [14]   F. Bullerjahn, M. Zajac and M. Ben Haha, "CSAB raw mix design: Effect on clinker formation and
487 reactivity," Materials and Structures, 2014.

488 [15]   S. Sahu, J. Havlica, V. Tomková and J. Majling, "Hydration behaviour of sulphoaluminate
489 Hydration behaviour of sulphoaluminate belite cement in the presence of various calciumsulphates,"
490 Thermochim. Acta, vol. 175, pp. 45-52, 1991.

491 [16]   F. Winnefeld and S. Barlag, "Influence of calcium sulfate and calcium hydroxide on the hydration
492 of calcium sulfoaluminate clinker," ZKG INTERNATIONAL, vol. 12, pp. 42-53, 2009.

493 [17]   F. Bullerjahn, D. Schmitt and M. Ben Haha, "Effect of raw mix design and of clinkering process on
494 the formation and mineralogical composition of (ternesite) belite calcium sulphoaluminate ferrite
495 clinker," Cement and Concrete Research, vol. 59, no.
496 http://dx.doi.org/10.1016/j.cemconres.2014.02.004, pp. 87-95, 2014.

497 [18]   L. Zhang and F. Glasser, " Hydration of calcium sulfoaluminate cement at less than 24 h,"
498 Advanced Cement Research., vol. 14, no. 4, p. 141–155, 2002.

499 [19]   V. Morin, G. Walenta, E. Gartner, P. Termkhajornkit, I. Baco and J. Casabonne, "Hydration of a
500 Belite-Calcium Sulfoaluminate-Ferrite cement : AetherTM," in International Congress on the Chemistry of
501 Cement, Madrid, Spain , 2011.

502 [20]   G. Li, G.Walenta and E. Gartner, "Formation and hydration of lowCO2 cements based on belite,
503 calcium sulfoaluminate and calcium aluminoferrite," in 12th International Congress on the Chemistry of
504 Cement, Montrea, Canadal, 2007.

505 [21]   L. Zhang and F. Glasser, "Investigation of the microstructure and carbonation of CS$\overline{A}$ - based
506 concretes removed fromservice," Cement and Concrete Research, vol. 35, no. 12, p. 2252–2260, 205.

507 [22]   K. Quillin, "Performance of belite-sulfoaluminate cements," Cement and Con crete Research, vol.
508 31, pp. 1341 - 1349, 2001.

509 [23]   M. Alesian, I. Pirazzoli, B. Maraviglia and F. Canonico, "NMR and XRD Study on Calcium
510 Sulfoaluminate Cement," Applied Magnetic Resonance, vol. 35, no. 1, pp. 33-41 , 2008.

511 [24]   J. Cheung, A. Jeknavorian, L. Roberts and D. Silva, "Impact of admixtures on the hydration
512 kinetics of Portland cement," Cement and Concrete Research, vol. 41, p. 1289–1309, 2011.

513 [25]   W. H. F. Taylor, Cement Chemistry, Chapter 10, pp 330-331, London: Academic Press Limited,
514 1990.

515 [26]   L. Pelletier, F. Winnefeld and B. Lothenbach, "Hydration mechanism and strength development
516 of the ternary Portland cement–calcium sulfoaluminate cement–anhydrite," in 17th Internationale
517 Baustofftagung (ibausil), Weimar, Germany, 2009.

518 [27]   L. Pelletier, F. Winnefeld and B. Lothenbach, "The ternary system Portland cement–calcium
519 sulphoaluminate clinker–anhydrite: hydration mechanism and mortar properties," Cement and Concrete
520 Research, vol. 32, pp. 497-507, 2010.

521 [28]   L. Pelletier-Chaignat, F. Winnefeld, B. Lothenbach, G. L. Saout, C. J. Mülle and C. Famy, "Influence
522 of the calcium sulphate source on the hydration mechanism of Portland cement–calcium
523 sulphoaluminate clinker–calcium sulphate binders," Cement & Concrete Composites, vol. 33, p. 551–561,
524 2011.

525 [29]   A. Cody, H. Leeb, R. Codya and P. Spry, "The effects of chemical environment on the nucleation,
526 growth, and stability of ettringite [Ca3Al(OH)6]2(SO4)326H2O," Cement and Concrete Research, vol. 34,
527 p. 869–881, 2004.

528 [30]   M. R. Nilforoushan and H. J. Sharp, "The effect of additions of alkaline-earth metal chlorides on
529 the setting behaviour of a refractory calcium aluminate cement," Cement and Concrete Research, vol.
530 25, pp. 1523-1534, 1995.

531 [31]   Z. Huaxin, L. Jiaping, L. Jianzhong and L. Changfeng, "HYDRATION HARDENING PROCESS
532 CONTROL TCHNOLOGY OF LOW ALKALINITY SULPHOALUMINATE CEMENT," in Second International
533 Conference on Microstructural-related Durability of Cementitious Composites, Amsterdam, The
534 Netherlands, 2012.

535 [32]   D. A. Kulik, T. Wagner, S. V. Dmytrieva, G. Kosakowski, F. F. Hingerl, K. V. Chudnenko and U. R.
536 Berner, "GEM-Selektor geochemical modeling package: revised algorithm and GEMS3K numerical kernel
537 for coupled simulation codes," Computational Geosciences, vol. 17, no. 1, pp. 1-24, 2012.

538 [33]   T. Thoenen and D. Kulik, "Nagra/PSI chemical thermodynamic database 01/01 for GEMS-selektor
539 (V.2-PSI) geochemical modellingmodelling code," http://gems.web.psi.ch/doc/pdf/TM-44-03-04-web.pdf
540 PSI, 2013.

541 [34]   W. Hummel, U. Berner, E. Curti, F. Pearson and T. Thoenen, "Nagra/PSI Chemical
542 Thermodynamic Data Base 01/01, USA also published as Nagra Technical Report NTB 02-16,," in
543 Universal Publishers/uPUBLISH.com, Wettingen, Switzerland 2002, 2002.

544 [35]   B. Lothenbach and F. Winnefeld, " Thermodynamic modelling of the hydration of Portland
545 cement," Cement and Concrete Research, vol. 36, p. 209–226, 2006.

546 [36]   T. Matschei, B. Lothenbach and F. Glasser, "Thermodynamic properties of Portland cement
547 hydrates in the system CaO–Al2O3–SiO2–CaSO4–CaCO3–H2O," Cement and Concrete Research, vol. 37,
548 pp. 1379-1410, 2007.

549 [37]   B. Lothenbach, G. L. Saout, E. Gallucci and K. Scrivener, "Influence of limestone on the hydration
550 of Portland cements," Cement and Concrete Research, vol. 38, pp. 848-860, 2008.

551 [38] H. Minard, S. Garrault, L. Regnaud and A. Nonat, "Mechanisms and parameters controlling the
552 tricalcium aluminate reactivity in the presence of gypsum," Cement and Concrete Research, vol. 37, p.
553 1418–1426, 2007.

554 [39] S. Pourchet, L. Regnaud, J. Perez and A. Nonat, "Early C3A hydration in the presence of different
555 kinds of calcium sulfate," Cement and Concrete Research, vol. 39, 2009.

556 [40] A. Demribas and S. Karshloglu, "The effect of boric acid sludges containing borogypsum on
557 properties of cement," Cement and Concrete Research, vol. 25, p. 1381–1384, 1995.

558 [41] L. Csetenyi and F. Glasser, "Borate retardation of cement set and phase relations in the system
559 Na2O–CaO–B2O3–H2O," Advancement in Cement Research, vol. 7, no. 25, p. 13–19, 1995.

560 [42] F. Venema, J. Peters and H. Van Bekkum, "Multinuclear magnetic resonance study of the
561 7coordination of aluminum(III) with tartaric acid in aqueous solution," Inorganica Chimica Acta , vol.
562 191(2), pp. 261-270, 1992 .

563 [43] M. Bishop and A. R. Barron, "Cement Hydration Inhibition with Sucrose, Tartaric Acid, and
564 Lignosulfonate: Analytical and Spectroscopic Study," Industrial & Engineering Chemistry Research , vol.
565 45, p. 7042–7049, 2006.

566 [44] J. Plank, P. Chatziagorastou and C. Hirsch, "New model describing distribution of adsorbed
567 superplasticizer on the surface of hydrating cement grain," J Build, vol. 10, pp. 9-13, 2007.

568 [45] A. Zingg, F. Winnefeld, L. Holzer, J. Pakusch, S. Becker and L. Gauckler, "Adsorption of
569 polyelectrolytes and its influence on the rheology, zeta potential, and microstructure of various cement
570 and hydrate phases," J Colloid Interf Sci, vol. 323, p. 301–12, 2008.

571 [46] J. Wolska and M. Bryjak, "Methods for boron removal from aqueous solutions — A review,"
572 Desalination, vol. 310, pp. 18-24, 2013.

573 [47] G. Li, P. L. Bescop and a. M. Moranville, "THE U PHASE FORMATION IN CEMENT-BASED SYSTEMS
574 CONTAINING HIGH AMOUNTS OF Na2SO4," Cement and Concrete Research, vol. 26, pp. 27-33, 1996.

575 [48] G. Li, P. L. Bescop and M. Moranville, "EXPANSION MECHANISM ASSOCIATED WITH THE
576 SECONDARY FORMATION OF THE U PHASE IN CEMENT-BASED SYSTEMS CONTAINING HIGH AMOUNTS
577 OF Na2SO4," Cement and Concrete Research,, vol. 26, pp. 195-201,, 1996.

578 [49] L. Fernandez-Carrasco, F. Puertas, M. Blanco-Varela and T. Va´zquez, "Potassium Dawsonite
579 Formation in Calcium Aluminate Cements," in International Conference on Calcium Aluminate Cements,
580 Heriot-Watt University, Edimburg, UK, 2001.

581 [50] L. Fernandez-Carrascoa, F. Puertasb, M. Blanco-Varelab, T. Vazquezb and J. Riusa, "Synthesis and
582 crystal structure solution of potassium dawsonite: An intermediate compound in the alkaline hydrolysis
583 of calcium aluminate cements," Cement and Concrete Research, vol. 35, p. 641–646, 2005.

584   [51]   S. E.C., F. J.R., W. J.L. and H. S.L., "Properties of carbonate-containing aluminum hydroxide
585   produced by precipitation at constant pH," J Pharm Sci. , vol. 73, no. 7, pp. 967-973, 1984.

586   [52]   H. G., "Process for producing dawsonite.," US Patent 5,078,983, 1992.

587   [53]   Z. X., W. Z., G. Z., X. X. and L. Z, "Hydrothermal synthesis and thermodynamic analysis of
588   dawsonite-type com pounds," J. Solid State Chem, vol. 177, p. 849–855, 2004.

589   [54]   P. Benezeth, D. A. Palmer, L. M. Anovitz and J. Horita, "Dawsonite synthesis and reevaluation of
590   its thermodynamic properties from solubility measurements: Implications for mineral trapping of CO2,"
591   Geochimica et Cosmochimica Acta, vol. 71, p. 4438–4455, 2007.

592   [55]   G. Stoica and J. Perez-Ramırez, "Stability and inter-conversion of synthetic dawsonites in
593   aqueous media," Geochimica et Cosmochimica Acta, vol. 74, p. 7048–7058, 2010.

594   [56]   M. Zajac, A. Rossberg, G. Le Saout and B. Lothenbach, "Influence of limestone and anhydrite on
595   the hydration of Portland cements," Cement and Concrete Composites, vol. 46, p. 99–108 , 2014.

596   [57]   N. L. Thomas and J. D. Birchall, "The retarding action of sugars on cement hydration," Cement
597   and Concrete Research, vol. 13, p. 830–842, 1983.

598   [58]   K. Luke and G. Luke, "Effect of sucrose on retardation of Portland cement," Advenacec Cement
599   Research, vol. 12, p. 9–18, 2000.

600   [59]   L. H. Zhang, L. J. J. Catalan, R. J. Balec, A. C. Larsen, H. H. Esmaeili and S. D. Kinrade, "Effects of
601   saccharide set retarders on the hydration of ordinary Portland cement and pure tricalcium silicate,"
602   Journal of American Ceramic Society, vol. 93, p. 279–287, 2010.

603   [60]   J.-P. Perez, "The mechanism of action of sodium gluconate on the fluidity and set of Portland
604   cement," in Proceedings of the 12th International Congress on the Chemistry of Cement, Montreal, 2007,
605   Montreal, Canada, 2007.

606   [61]   B. J. Smith, L. R. Roberts, G. P. Funkhouser, V. Gupta and B. F. Chmelka, "Reactions and Surface
607   Interactions of Saccharides in Cement Slurries," Langmuir, vol. 28, p. 14202–14217, 2012.

608   [62]   D. Rossiter, D. Ilievski, P. Smith and G. Parkinson, "The mechanism of sodium gluconate
609   poisoning of gibbsite precipitation," Chemical Engineering Research and Design, vol. (A7) 74, pp. 828 -
610   834, 1996.

611   [63]   D. Rossiter, D. Ilievski, P. Smith and G. Parkinson, "Investigation of the unseeded nucleation of
612   gibbsite, Al(OH)3, from synthetic bayer liquors," Journal of Crystal Growth, vol. 191, p. 525, 1998.

613   [64]   A. Pallagi, P. Sebok, P. Forgó, T. Jakusch, I. Pálinkó and P. Sipos, "Multinuclear NMR and
614   molecular modelling investigations on the structure and equilibria of complexes that form in aqueous
615   solutions of Ca2+ and gluconate," Carbohydrate Research, vol. 345, p. 1856–1864, 2010.

616 [65] A. Pallagi, Á. G. Tasi, G. Peintler, P. Forgo, I. Pálinkód and P. Sipos, "Complexation of Al(III) with
617 gluconate in alkaline to hyperalkaline solutions: formation, stability and structure," Dalton Transactions,
618 vol. 42, p. 13470–13476, 2013.

619 [66] T. Bechtold, E. Burtscher and A. Turcanu, "Ca2+–Fe3+–D-gluconate-complexes in alkaline
620 solution. Complex stabilities and electrochemical properties," Dalton Transactions, no. 13, p. 2683–2688,
621 2002.

622 **Tables**

623 **Table 1 Chemical composition of the investigated materials (wt.-%).**

Component	Cement clinker	AH
SiO_2	17.95	2.31
Al_2O_3	15.30	0.73
TiO_2	0.58	0.02
MnO	0.04	0.00
Fe_2O_3	3.26	0.25
CaO	51.88	38.04
MgO	1.09	1.49
K_2O	0.74	0.17
Na2O	0.13	0.00
SO_3	6.68	51.93
P_2O_5	0.20	0.02
$\sum$	98.77	98.62

624

625

626

627 **Table 2 Mineral composi on of the inves gated materials determined by the Rietveld analysis (wt.-%).**

Phase	Cement clinker	AH
$C_4A_3\bar{S}$	24.8	
β-C_2S	52.4	
C_4AF	6.6	
C_2F	2.1	
CA	1.2	
Cc (Calcite)	1.9	
$K\bar{S}$ (Ankarnite)	0.5	
$C_2K\bar{S}_3$ (Langbainite)	1.5	
$C\bar{S}$ (Anhydrite)	2.2	88.0
Dolomite		7.4
Other	6.8	4.6
∑	100.0	100.0

628

629

630 **Table 3 Experimental matrix in wt.-%.**

Sample	C	CAH	T	B	G
			W/C=2.0		
C	100				
CAH		100			
C-T	100		2		
C-B	100			2	
C-G	100				2
CAH-T		100	2		
CAH-B		100		2	
CAH-G		100			2

631

632

633

Table 4 Contents of anhydrous clinker phases, e ringite (Et) and XRD amorphous rela ve to the dry content in wt.-% determined by the XRD-Rietveld analysis (cement C).

	anhydrous	30 min	1 h	2 h	4 h	8 h	24 h	48 h	168 h
C									
C4A3S;⁻	24.8	20.3	20.4	20.7	16.2	3.0	0.0	-	0.0
C2S	52.4	47.3	48.1	50.5	43.7	39.3	35.4	-	27.7
C4AF	6.6	6.1	6.2	6.1	5.2	3.4	2.3	-	0.0
C2F	2.1	1.6	1.7	1.9	1.7	1.4	1.5	-	0.0
CA	1.2	0.7	0.7	0.8	0.7	0.3	0.0	-	0.0
Cc	1.9	1.4	1.3	1.4	1.1	0.7	0.1	-	0.0
CS;⁻	2.2	1.4	1.2	1.2	0.8	0.0	0.0	-	0.0
Et	0.0	5.0	5.6	7.7	8.4	15.0	15.6	-	14.8
XRD Amorphous	0.0	11.5	10.2	4.7	18.0	32.7	41.0	-	53.0
C-T									
C4A3S;⁻	24.8	24.7	24.8	24.7	24.4	17.3	13.7	-	0.0
C2S	52.4	51.3	52.5	52.9	51.8	43.2	43.4	-	25.4
C4AF	6.6	6.8	6.8	6.9	6.8	5.5	4.9	-	0.0
C2F	2.1	2.1	2.0	2.1	2.2	1.7	1.8	-	0.9
CA	1.2	1.0	0.9	1.0	0.8	0.6	0.4	-	0.0
Cc	1.9	1.6	1.7	1.5	1.5	1.2	1.1	-	0.2
CS;⁻	2.2	1.9	2.0	1.9	1.9	1.2	0.0	-	0.0
Et	0.0	0.0	0.0	0.0	0.0	5.7	11.1	-	19.9
XRD Amorphous	0.0	5.5	4.3	3.9	5.9	19.7	19.5	-	50.9
C-B									
C4A3S;⁻	24.8	24.3	23.5	24.0	23.9	24.0	23.6	0.0	0.0
C2S	52.4	50.1	49.3	50.7	49.7	50.6	49.1	33.0	30.5
C4AF	6.6	6.4	6.7	6.6	6.6	6.7	6.6	2.2	0.0
C2F	2.1	2.1	2.1	2.3	2.0	2.2	2.2	0.7	0.0
CA	1.2	0.9	0.8	0.7	0.9	0.7	0.8	0.2	0.0
Cc	1.9	1.5	1.6	1.6	1.6	1.4	1.5	0.0	0.0
CS;⁻	2.2	1.8	1.8	1.9	1.8	1.8	1.9	0.0	0.0
Et	0.0	0.0	0.0	0.0	0.0	0.0	0.0	17.4	14.8
XRD Amorphous	0.0	7.7	8.0	6.5	7.7	6.7	8.2	43.8	51.9
C-G									
C4A3S;⁻	24.8	24.1	24.3	24.1	22.4	21.3	18.1	-	11.0
C2S	52.4	49.6	49.6	50.2	46.4	47.9	44.2	-	42.0
C4AF	6.6	6.5	6.5	6.7	5.7	6.1	5.2	-	4.5
C2F	2.1	1.8	2.1	2.1	2.0	1.6	1.6	-	1.5
CA	1.2	0.6	0.8	0.8	0.7	0.6	0.6	-	0.5
Cc	1.9	1.5	1.5	1.5	1.5	1.3	1.2	-	1.0
CS;⁻	2.2	1.9	1.9	1.9	1.7	1.6	1.1	-	0.0
Et	0.0	0.0	0.0	0.0	1.8	4.6	6.8	-	11.6
XRD	0.0	9.0	8.5	7.9	13.2	10.6	17.1	-	23.5

Amorphous									

636

637

Table 5 Contents of anhydrous clinker phases, e ringite (Et) and XRD amorphous rela ve to the dry content in wt.-% determined by the XRD-Rietveld analysis (cement CAH).

	anhydrous	30 min	1 h	2 h	4 h	8 h	24 h	48 h	168 h
CAH									
C4A3S;⁻	22.3	18.4	20.1	16.4	3.7	0.0	0.0	-	0.0
C2S	47.2	41.0	47.8	40.9	36.3	35.6	35.0	-	28.5
C4AF	5.9	5.4	5.7	5.0	3.3	2.8	3.1	-	2.9
C2F	1.9	1.7	1.7	1.3	1.3	1.5	1.2	-	0.8
CA	1.1	0.7	0.6	0.5	0.3	0.3	0.1	-	0.0
Cc	11.1	1.2	1.2	1.1	0.8	0.8	0.8	-	0.9
CS;⁻	2.0	10.2	10.0	9.6	10.0	9.7	6.4	-	0.0
Et	0.0	4.9	6.0	7.7	22.9	29.2	31.9	-	32.2
XRD Amorphous	0.0	11.9	1.0	13.8	23.8	24.5	24.8	-	32.0
CAH-T									
C4A3S;⁻	22.3	21.3	21.4	21.3	22.1	18.1	11.4	-	0.0
C2S	47.2	45.1	45.4	44.4	45.9	44.2	39.6	-	31.7
C4AF	5.9	6.1	6.4	6.5	6.5	5.8	4.9	-	3.6
C2F	1.9	1.7	1.9	1.7	1.7	1.8	1.8	-	0.9
CA	1.1	0.8	0.8	0.8	0.5	0.4	0.3	-	0.0
Cc	1.7	1.4	1.5	1.5	1.4	1.3	1.2	-	0.7
CS;⁻	11.1	9.8	10.0	10.0	9.9	9.5	9.7	-	0.0
Et	0.0	0.0	0.0	0.0	0.0	3.8	11.6	-	36.6
XRD Amorphous	0.0	7.8	7.1	8.4	6.6	10.2	19.0	-	23
CAH-B									
C4A3S;⁻	22.3	21.8	22.3	21.9	21.2	21.4	20.8	0.0	0.0
C2S	47.2	45.7	46.6	45.2	45.1	43.9	43.4	32.4	31.8
C4AF	5.9	6.6	6.7	6.1	6.1	6.0	6.4	3.8	3.5
C2F	1.9	1.8	2.0	1.9	2.0	1.9	1.5	1.2	1.1
CA	1.1	0.7	0.6	0.6	0.6	0.5	0.6	0.3	0.1
Cc	1.7	1.5	1.6	1.5	1.4	1.5	1.4	0.8	1.1
CS;⁻	11.1	9.8	10.0	10.0	9.9	9.5	9.7	0.0	0.0
Et	0.0	0.0	0.0	0.0	0.0	0.0	0.0	26.5	25.8
XRD Amorphous	0.0	6.9	4.3	6.9	7.1	8.7	9.7	33.0	34.0
CAH-G									
C4A3S;⁻	22.3	21.8	21.2	21.2	20.1	19.0	17.1	-	8.5
C2S	47.2	44.9	43.9	44.5	42.6	42.0	41.6	-	36.8
C4AF	5.9	6.1	6.1	6.0	6.1	5.5	5.9	-	4.4
C2F	1.9	2.0	1.9	1.8	1.5	1.6	1.2	-	1.3
CA	1.1	0.5	0.8	0.5	0.6	0.4	0.6	-	0.3
Cc	1.7	1.5	1.4	1.5	1.4	1.3	1.4	-	1.0
CS;⁻	11.1	9.9	9.4	9.8	9.9	9.7	9.2	-	5.0
Et	0.0	0.0	0.0	0.0	0.0	3.9	7.0	-	13.0
XRD	0.0	8.4	9.7	8.7	12.3	11.7	10.9	-	25.3

Amorphous									

640

641

642

Table 1 Pore solu on chemistry of cements C measured by ICP (mmol/l) and pH electrode (-)

	5 min	30 min	1 h	2 h	4 h	8 h	24 h	48 h	168 h
C									
Ca	16.5	7.6	3.8	2.8	2.0	1.1	0.3	-	0.4
Si	0.01	0.01	0.01	0.01	0.01	0.01	0.01	-	0.01
Al	11.38	20.98	34.43	47.85	67.31	66.79	20.57	-	0.05
Na	11.9	12.7	12.5	11.6	12.0	15.1	15.5	-	17.8
K	80.3	78.3	78.8	78.3	78.8	56.8	54.2	-	62.1
Fe	0.01	0.01	0.01	0.01	0.01	0.01	0.01	-	0.01
S (sulphur)	49.2	35.9	26.4	18.1	7.3	1.6	1.3	-	0.1
pH	11.17	11.15	11.42	11.52	11.73	12.58	13.1	-	13.4
C-T									
Ca	28.8	28.4	27.1	25.5	22.7	4.3	1.6	-	0.5
Si	0.01	0.01	0.01	0.01	0.01	0.01	0.01	-	0.01
Al	0.03	0.01	0.01	0.04	0.04	39.81	77.09	-	1.06
Na	66.3	43.6	43.1	43.1	44.4	45.7	47.2	-	46.2
K	121.7	100.0	100.3	100.3	102.8	95.42	97.42	-	97.21
Fe	0.01	0.01	0.01	0.01	0.01	0.01	0.01	-	0.01
S (sulphur)	104.1	84.2	84.8	85.4	85.4	65.8	41.4	-	0.3
pH	11.7	11.9	12.0	12.1	12.2	11.5	12.1	-	13.5
C-B									
Ca	57.6	37.3	29.2	47.9	42.4	35.0	33.4	0.0	2.4
Si	0.74	0.01	0.01	1.03	0.99	0.34	0.01	0.01	0.01
Al	0.01	0.01	0.01	0.01	0.01	0.01	0.01	25.57	0.05
Na	15.0	13.4	13.1	15.4	15.4	16.6	16.5	73.5	25.0
K	58.8	71.4	68.3	58.6	58.8	53.2	52.4	65.5	63.2
Fe	0.01	0.01	0.01	0.01	0.01	0.01	0.01	0.01	0.01
S (sulphur)	81.1	65.8	43.0	65.8	60.8	60.8	55.0	1.7	0.1
B	122.2	111.1	94.4	75.9	85.2	72.2	59.3	<0.1	0.5
pH	8.5	8.6	8.9	8.9	9.1	9.6	11.0	13.3	13.3
C-G									
Ca	48.1	28.1	24.1	22.5	23.9	11.6	7.5	-	2.6
Si	0.01	0.59	0.01	0.01	1.31	0.01	0.01	-	0.01
Al	2.98	1.88	1.78	1.52	13.45	32.65	43.51	-	88.95
Na	80.6	56.9	56.7	57.0	62.7	69.5	65.1	-	54.5
K	80.8	70.3	70.6	70.6	71.9	63.9	61.9	-	61.9
Fe	0.10	0.07	0.06	0.06	0.37	0.52	0.67	-	0.50
S (sulphur)	111.6	75.5	75.1	75.5	73.9	68.0	55.8	-	18.8
pH	11.8	11.9	12.0	12.1	11.7	11.7	11.8	-	12.0

669   **Table 2 Pore solu on chemistry of cements CAH measured by ICP (mmol/l) and pH electrode (-)**

|	5 min	30 min	1 h	2 h	4 h	8 h	24 h	48 h	168 h
CAH									
Ca	17.5	9.7	6.9	4.3	0.8	0.3	0.2	-	0.3
Si	0.01	0.01	0.01	0.01	0.01	0.01	0.01	-	0.01
Al	11.01	21.09	22.31	31.13	53.45	24.83	22.57	-	8.23
Na	13.1	14.9	14.8	13.5	15.4	15.4	14.7	-	14.7
K	56.5	2.9	65.9	55.2	58.8	50.4	52.2	-	48.8
Fe	0.01	0.01	0.01	0.01	0.01	0.01	0.01	-	0.01
S (sulphur)	52.8	44.3	29.7	22.5	9.4	18.3	6.8	-	1.6
pH	11.1	11.0	11.1	11.4	11.9	12.3	12.8	-	13.0
CAH-T									
Ca	27.1	23.3	22.4	22.6	21.3	5.7	2.6	-	0.2
Si	0.60	0.79	0.73	0.83	0.56	0.01	0.01	-	0.01
Al	0.01	0.01	0.01	0.01	0.01	36.84	36.06	-	64.60
Na	39.8	41.5	42.4	42.5	42.4	56.1	46.5	-	45.2
K	82.4	102.0	101.8	78.3	76.7	87.0	85.9	-	77.5
Fe	0.01	0.01	0.01	0.01	0.01	0.01	0.01	-	0.01
S (sulphur)	79.5	79.2	84.5	80.4	83.3	74.2	68.6	-	19.6
pH	11.8	11.9	12.0	12.1	12.2	11.4	11.5	-	12.9
CAH-B									
Ca	61.9	57.1	52.6	49.2	43.8	37.5	35.1	0.1	0.1
Si	0.01	0.60	0.44	0.42	0.27	0.41	0.54	0.01	0.01
Al	0.01	0.01	0.01	0.01	0.01	0.01	0.01	20.00	9.64
Na	14.1	13.4	13.4	13.4	13.7	18.7	16.2	70.9	27.6
K	48.5	63.9	63.7	63.7	63.7	53.2	50.7	53.7	46.0
Fe	0.01	0.01	0.01	0.01	0.01	0.01	0.01	0.01	0.01
S (sulphur)	83.6	64.9	61.5	58.4	52.9	67.0	55.5	43.0	12.4
B	131.5	118.5	114.8	100	88.9	74.1	63	<0.1	0.9
pH	8.5	8.6	8.7	8.9	9.1	9.5	10.5	12.9	12.9
CAH-G									
Ca	52.1	40.8	36.9	32.5	32.4	11.8	8.8	-	4.1
Si	0.27	1.11	1.67	0.96	0.15	0.01	0.01	-	0.01
Al	2.87	1.71	1.59	1.54	2.49	29.17	35.03	-	32.39
Na	50.4	56.9	50.1	50.4	50.3	80.3	66.7	-	54.2
K	48.8	64.7	52.7	49.3	53.5	60.4	60.4	-	54.7
Fe	0.10	0.06	0.07	0.06	0.08	0.44	0.59	-	0.90
S (sulphur)	98.8	72.7	87.9	82.3	82.0	71.7	62.7	-	52.4
pH	11.8	12.0	12.0	12.1	12.2	11.7	11.6	-	11.4

670

671

672   **Figures**

673
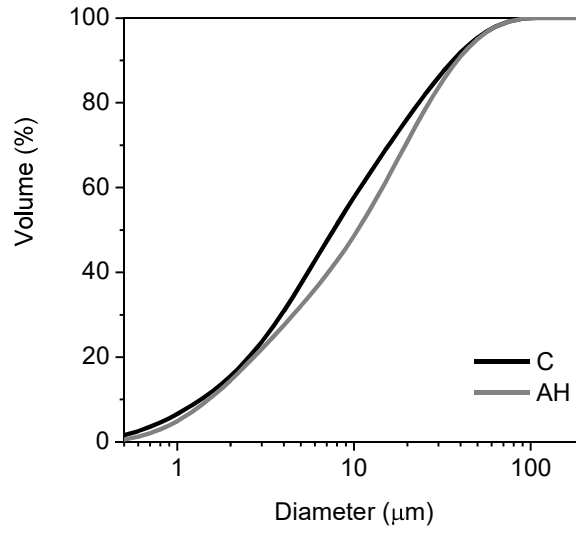
674

675   **Figure 1. Par cle size distribu on of C and AH determined by laser di rac on.**
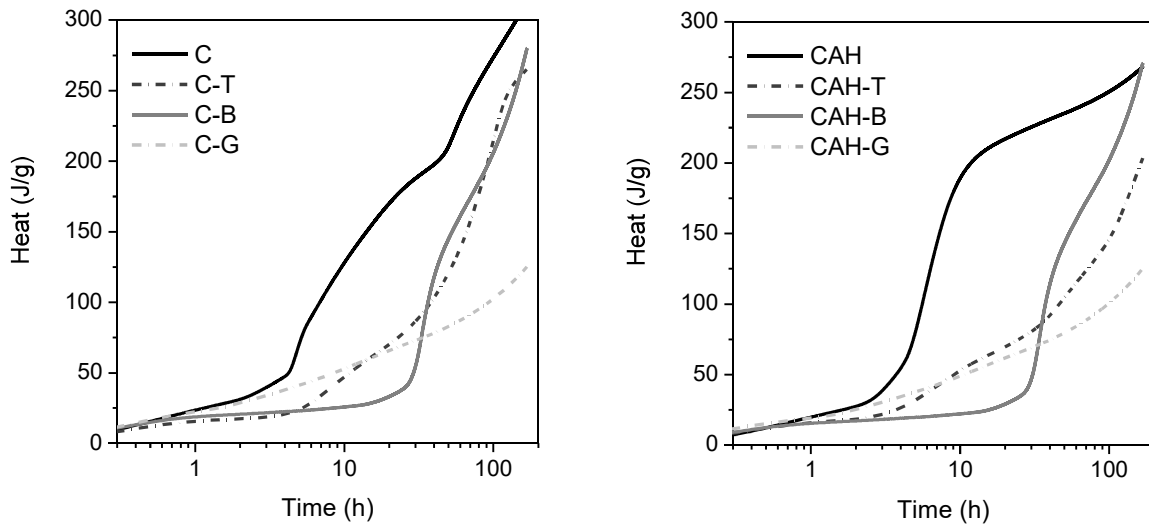
676
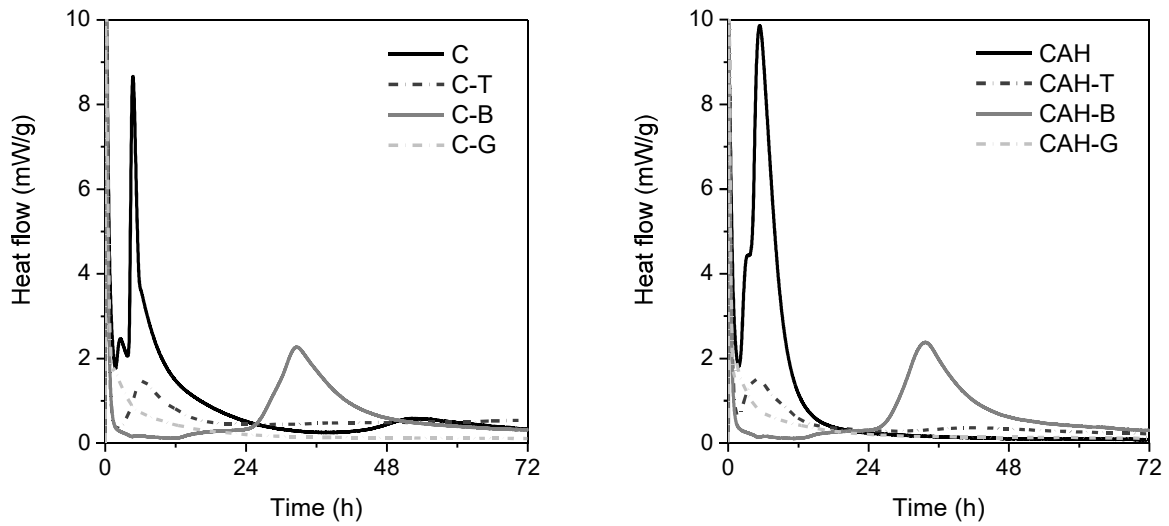
677   **Figure 2. Heat ow of the inves gated samples within the rst 72 hours.**
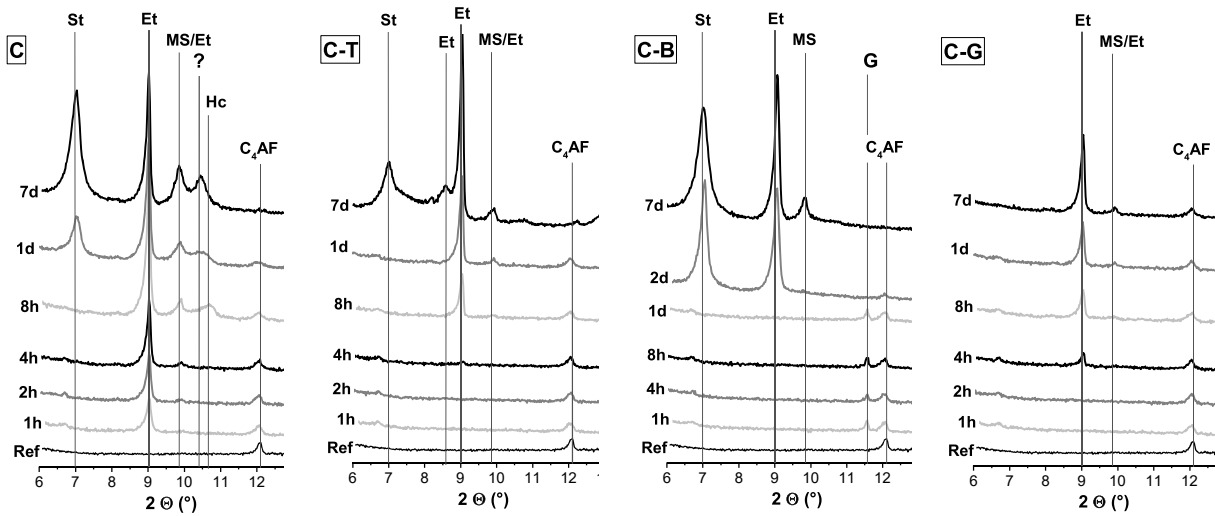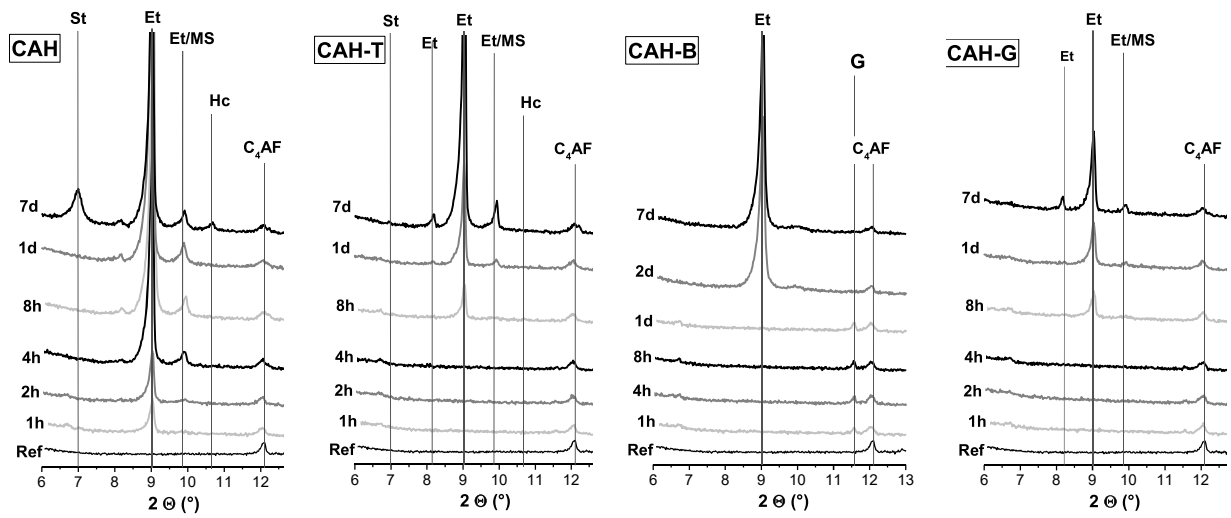
678

679   Figure 3. Cumulative heat of the investigated samples during the first 7 days of hydration.

680

681

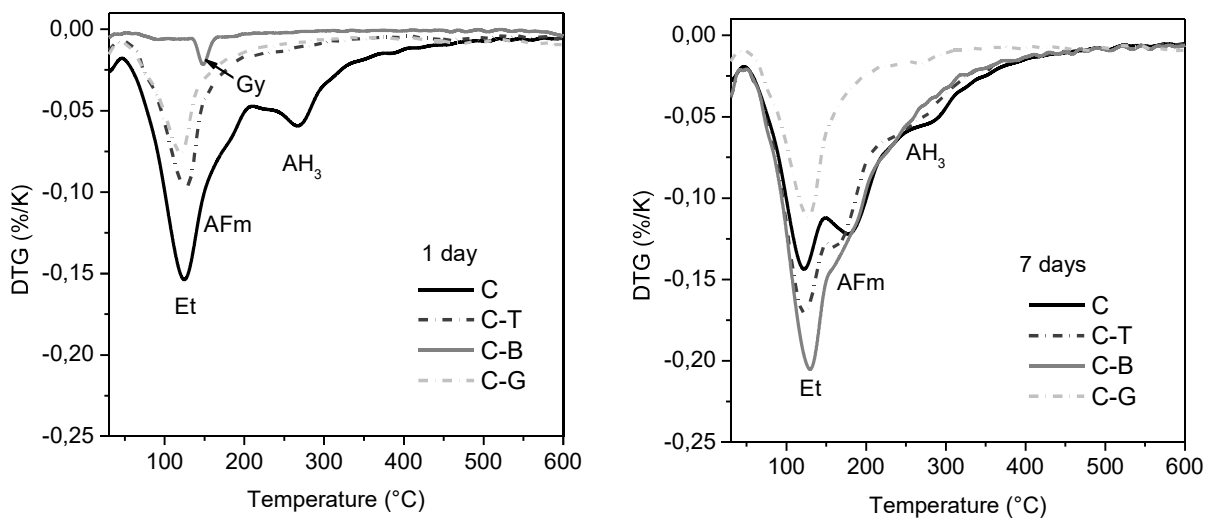682   Figure 4. Comparison of XRD plots for investigated C cements

683 Figure 5. Comparison of XRD plots for inves gated CAH cements

684

685

686 Figure 6. Comparison of the DTG plots at 1 and 7 days for the C samples (Et – e ringite, AFm – monophases and
687 strätlingite, AH_3 – aluminium hydroxide, Gy - gypsum

688
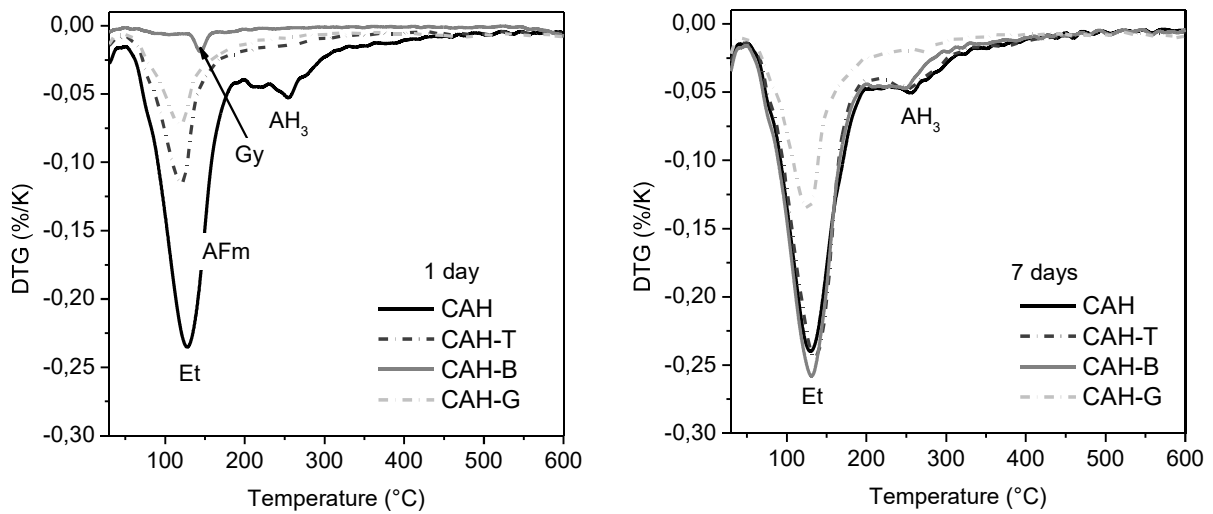
Figure 7. Comparison of the DTG plots at 1 and 7 days for the CAH samples (Et – e ringite, AFm – monophases and strätlingite, AH_3 – aluminium hydroxide, Gy - gypsum).
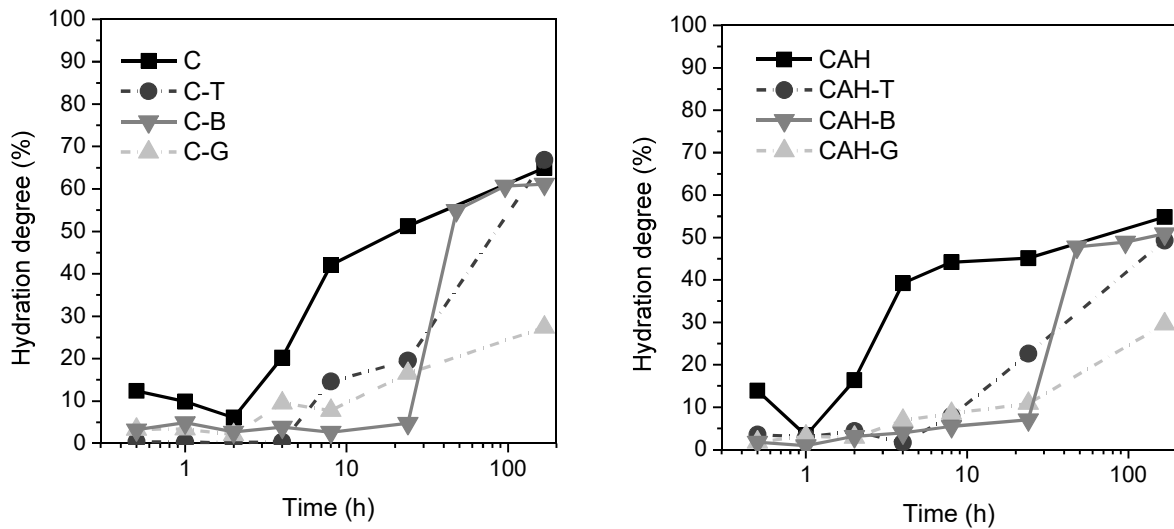
Figure 8. Hydra on degree of cement clinker calculated as a sum of dissolu on degrees of clinker minerals ($C_4A_3\$+C_2S+C_4AF+C_2F+CA$) . Calcula ons are based on the Rietveld analysis of the XRD measurements (Error! Reference source not found. **and** Error! Reference source not found.**).**

697
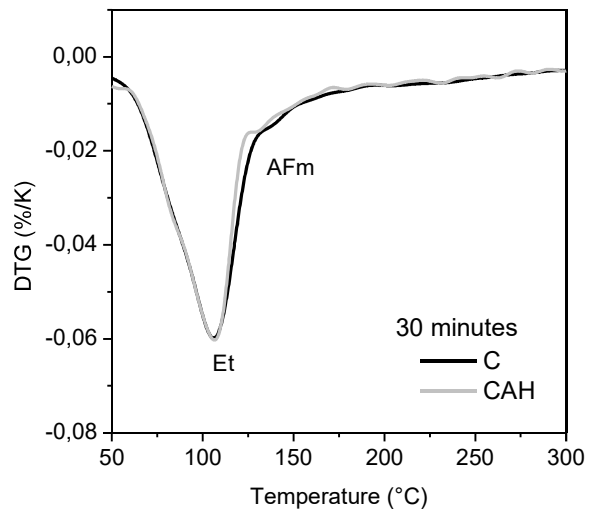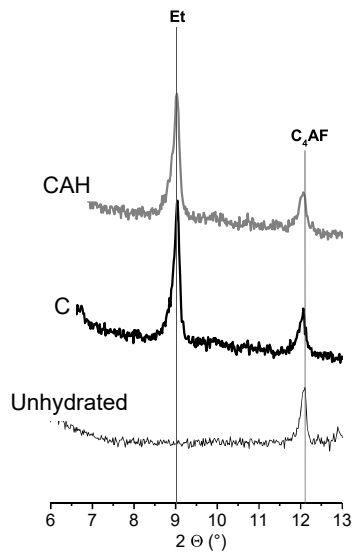
Figure 9. DTG and XRD data for C and CAH samples a er 30 minutes of hydra on.

699

700

701
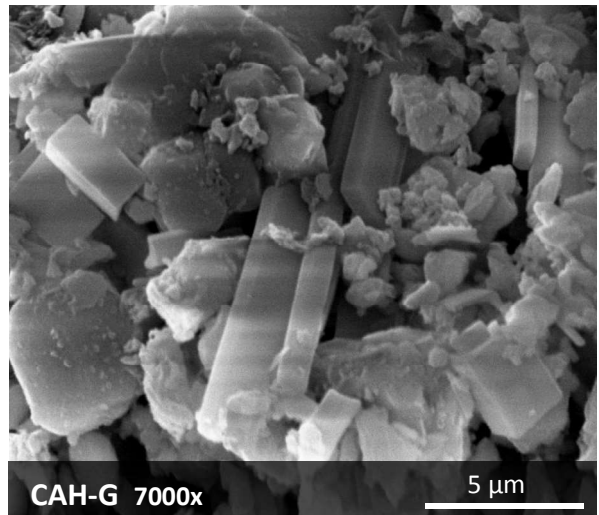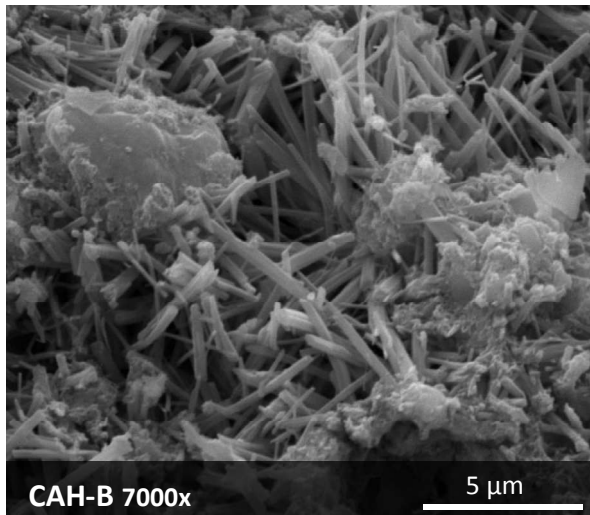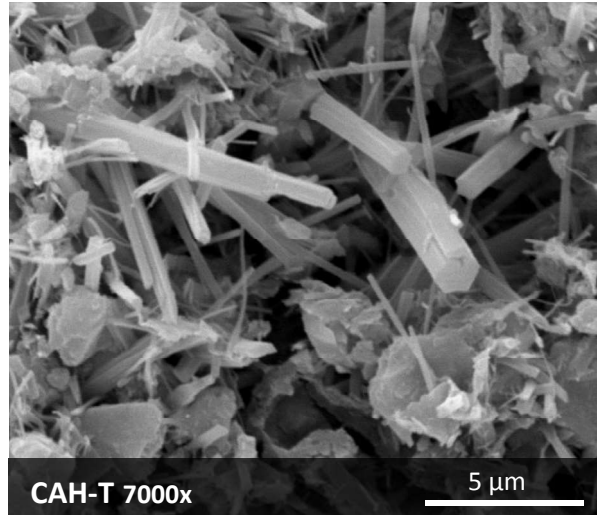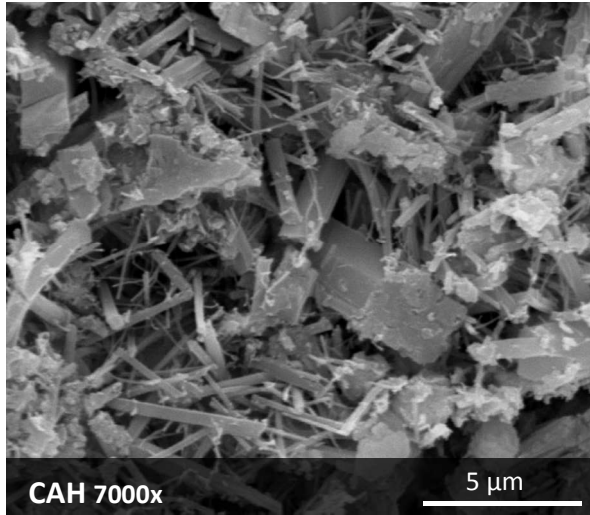
702   **Figure 10. SEM images of fractured surfaces a   er 1 day of hydra   on (W/C of 0.5).**
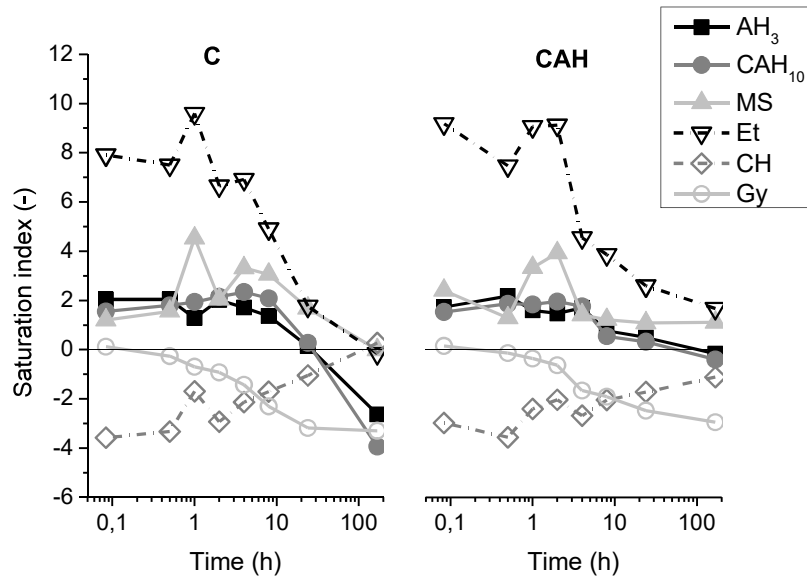
703

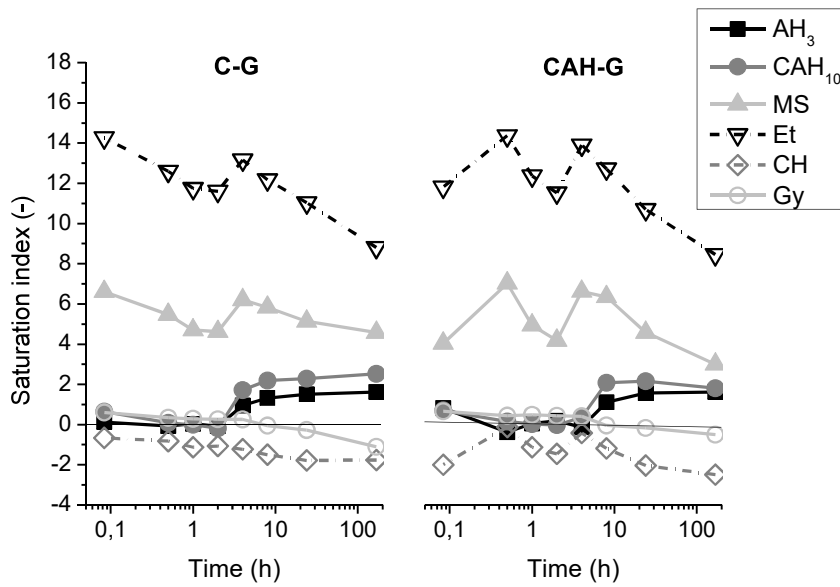Figure 11. Satura on indices calculated from the pore solu on concentra ons of C and CAH sample.
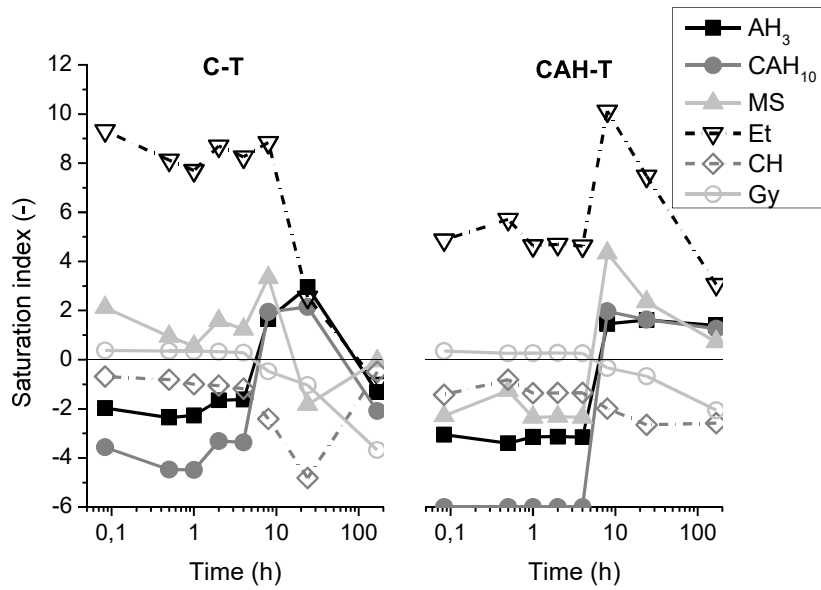
705

Figure 12. Satura on indices calculated from the pore solu on chemistry of C-T and CAH-T samples. If the concentra on of Al was not measurable, the detec on limit of 0.01 mmol/l was used for the calcula ons. The e ect of tartrate was neglected.
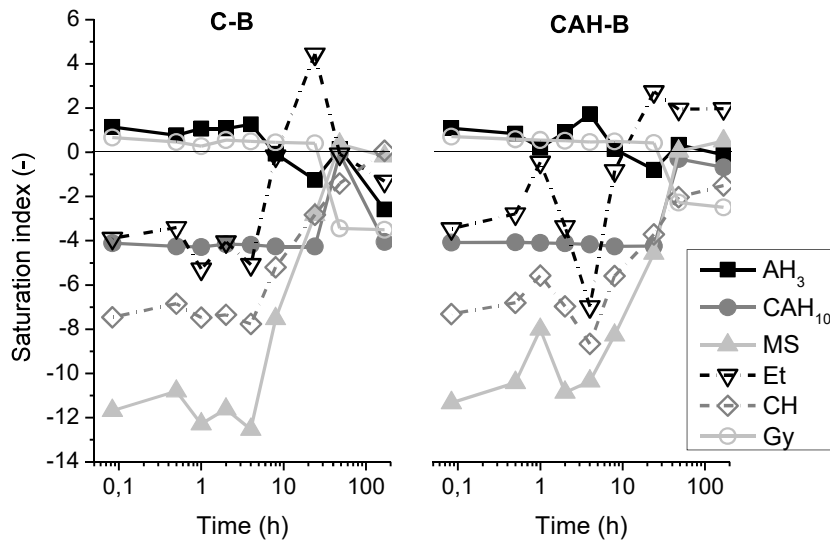
709

Figure 13. Satura on indices calculated from the pore solu on chemistry of C-B and CAH-B sample. If the concentra on of Al was not measurable, the detec on limit of 0.01 mmol/l was used for calcula ons.
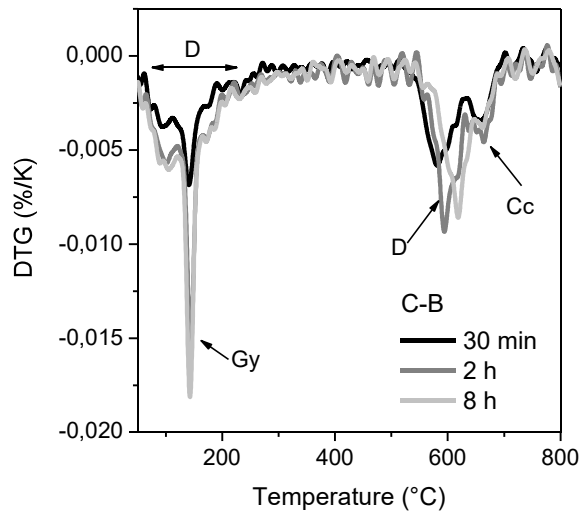

712

Figure 14. Satura on indices calculated from the pore solu on chemistry of C-G and CAH-G sample. If the concentra on of Al was not measurable, the detec on limit of 0.01 mmol/l was used for calcula ons.
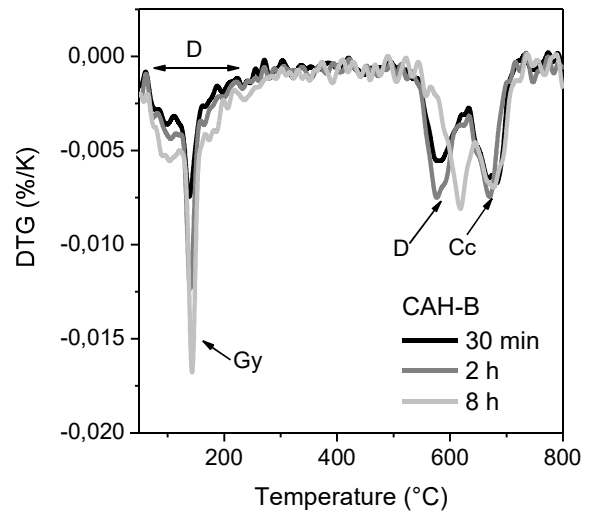
Figure 15. DTG curves of C-B and CAH-B at early   mes, D – Dawsonite.